Journal of Zhejiang University-SCIENCE A (Applied Physics & Engineering) 2023 24(10):886-897
www.jzus.zju.edu.cn; www.springer.com/journal/11582
E-mail: jzus_a@zju.edu.cn

Research Article

https://doi.org/10.1631/jzus.A2200571

Effect of CO_2-mixing dose and prolonged mixing time on fresh and hardened properties of cement pastes

Minlu WANG, Shuang LUO, Ba Tung PHAM, Tung-Chai LING✉

College of Civil Engineering, Hunan University, Changsha 410082, China

Abstract: This study aims to investigate the influence of CO_2-mixing dose (mass fractions of 0.3%, 0.6%, and 0.9%) and prolonged mixing time on the fresh and hardened properties of cement pastes. The CO_2-mixing can act as coagulant in fresh cement mixtures, resulting in a significant reduction in workability associated with the formation of a rich calcium carbonate network on the surface of cement particles. The CO_2-mixing cement pastes were found to be much stiffer and more difficult to handle, place, and compact than the control mixture, which had a negative effect on the mechanical strength performance of the hardened pastes. However, prolonging the mixing time for 1 min (immediately after CO_2-mixing) can effectively improve the workability (by ~53%–85%) by breaking up the flocculation network of deposited calcium carbonates. As a result, the presence of detached calcium carbonate accelerated early cement hydration and densified the microstructure; this improved early-age compressive strength by ~6%–32%, depending on the CO_2-mixing dose used. Therefore, it seems that the CO_2-mixing dose should be controlled at ≤0.6% with the mixing time prolonged in order to attain satisfactory workability and mechanical strength.

Key words: CO_2-mixing; Calcium carbonate; Early cement hydration; Flowability; Microstructure

1 Introduction

Accelerated carbonation (or CO_2 curing) has been extensively studied for its potential to improve the mechanical strength of cement concrete and reduce its environmental impact (Ashraf, 2016). However, special conditions including temperature, pressure, CO_2 concentration, and sophisticated equipment are required for an accelerated carbonation process, and in general the approach can only be applied in precast production (Zhang et al., 2017). In addition, CO_2 can be sequestrated into cement-based materials and solid waste under aqueous conditions (Li et al., 2023; Mehdizadeh et al., 2023). Both dry and aqueous carbonation methods require a long process for the carbonation reaction (hours or days). Recently, the application of CO_2-mixing by directly mixing CO_2 with fresh ready-mix concrete has attracted a lot of attention due to the short reaction time (a few minutes during mixing) and its feasibility for wider application in the concrete industry. According to (Monkman and MacDonald, 2016; Monkman et al., 2016), the amount of CO_2 incorporated (~0.05%–1.5%) during concrete mixing or batching has a significant influence on compressive strength. CO_2 can convert calcium minerals into very fine calcium carbonate ($CaCO_3$) with a size of ~70 nm that acts as nucleation sites to accelerate cement hydration (Monkman et al., 2020). Monkman and MacDonald (2017) claimed that the cement consumption for a given designed concrete strength was reduced by ~5%–8%. The reaction between CO_2 and cement clinkers (including C_3S and C_2S for the precipitation of $CaCO_3$ in the presence of water) can be expressed by Eqs. (1) and (2) (Berger et al., 1972).

$$3(3CaO\cdot SiO_2)+(3-x)CO_2+yH_2O\rightarrow xCaO\cdot SiO_2\cdot yH_2O+(3-x)CaCO_3, \quad (1)$$

$$2(2CaO\cdot SiO_2)+(2-x)CO_2+yH_2O\rightarrow xCaO\cdot SiO_2\cdot yH_2O+(2-x)CaCO_3. \quad (2)$$

In terms of workability performance, Monkman and MacDonald (2016) and Liu et al. (2021) reported that CO_2-mixing of a fresh concrete mixture dramatically

✉ Tung-Chai LING, tcling@hnu.edu.cn, tcling611@yahoo.com
Tung-Chai LING, https://orcid.org/0000-0002-8276-5212

Received Nov. 28, 2022; Revision accepted Mar. 28, 2023;
Crosschecked Sept. 20, 2023

reduces workability. To solve this technical problem, Monkman and MacDonald (2016) used extra water to maintain equal workability of the concrete mixture and were able to successfully enhance the compressive strength by ~10%–30% compared to the control mixture. Liu et al. (2021) used superplasticizers to refine the flowability of CO_2-mixed cement paste and attained comparable strength to that of the control sample. Lippiatt et al. (2019) used a saturated aqueous CO_2 solution as mixing water for the preparation of cement pastes and found that the presence of an aqueous CO_2 solution (carbonic acid) in the paste greatly reduced flowability (Kwasny et al., 2014; Lippiatt et al., 2019; Lippiatt and Ling, 2020). In comparison to an enclosed mixing environment, the reduction of workability associated with the CO_2-mixing approach was even more pronounced (Liu, 2019). Luo et al. (2022) used fly ash to replace 10%–20% of cement in order to improve the workability of CO_2-mixed cement pastes due to the material's spherical morphology, and obtained an ~15% increase in strength. However, the mechanism of flocculation and breakup of the deposited calcium carbonate on the surface of the cement particles after subjection to prolonged mixing time was not clear.

Generally, increasing cement-mixing speed, intensity, and time enables great enhancement of the rheological behavior, hydration, and microstructure of cement concrete (Han and Ferron, 2015, 2016). According to Zhao et al. (2022), prolonging vibratory mixing helps to break down flocculation of cement particles and produce better fluidity in the concrete mixture. In fact, prolonging a short mixing period can improve the uniformity and consistency of fresh concrete, especially in the case of high-stiffness mixtures (Urban and Sicakova, 2018). In contrast to mixing at an ambient temperature (25 °C), prolonging mixing time at 40 °C for 60, 120, and 180 min can better improve the compressive strength of concrete (Hossain et al., 2018). It can be suggested that increased mixing time is anticipated to alter the fresh and hardened properties of cement pastes, in particular with additional admixture or filler, and this could also apply for the introduction of CO_2 in fresh cement paste.

This paper studies the influence of further mixing (applied immediately after CO_2-mixing with mass fractions of 0.3%, 0.6%, and 0.9%) on the fresh and hardened properties of cement pastes. All the cement pastes were prepared with a fixed water-to-cement (w/c) ratio of 0.5 in an enclosed (airtight) mixer. Calcium carbonate precipitation was confirmed by thermogravimetric analysis (TGA) and scanning electron microscope (SEM) with an energy-dispersive spectrometer (EDS). The porosity was quantified using backscattered electron microscopy (BSE) techniques. The kinetics of cement hydration with and without CO_2-mixing were investigated through isothermal calorimetry.

2 Experimental

2.1 Materials

Ordinary Portland cement (OPC) with a strength grade of P.I. 42.5 and deionized pure water were used to prepare cement pastes. The chemical and mineral compositions of OPC are given in Tables 1 and 2, respectively. CO_2 gas with an industrial-grade purity of 99% (volume fraction) was obtained from Rizhen Industrial-Gas Manufacturer in Changsha, China.

Table 1 Chemical composition of OPC

Chemical composition	Mass content (%)	Chemical composition	Mass content (%)
CaO	63.43	Fe_2O_3	3.99
SiO_2	20.30	MgO	2.03
Al_2O_3	5.42	SO_3	0.97

Table 2 Mineral composition of OPC

Mineral composition	Mass content (%)	Mineral composition	Mass content (%)
C_3S	58.99	C_4AF	12.13
C_2S	14.02	Gypsum	2.09
C_3A	7.62	Other	5.15

2.2 Mixing process and sample preparation

The CO_2-mixing cement pastes were prepared with a fixed w/c ratio of 0.5; the mix design is shown in Table 3. Based on Eq. (3), volumetric flow rates were determined for each mix design of CO_2-mixing cement pastes (mass fractions of 0.3%, 0.6%, and 0.9%).

$$v=\frac{m_{CO_2}}{\rho_{CO_2}\times t}, \tag{3}$$

where v is the CO_2 gas-flow rate (L/min), m_{CO_2} is the mass of injected CO_2 gas (g), ρ_{CO_2} is the density of CO_2

Table 3 Mix design of CO_2-mixing cement pastes

Sample	OPC mass (g)	Water mass (g)	w/c ratio	CO_2 dose* (%)	m_{CO_2} (g)	Flow rate (L/min)
AM	1500	750	0.5	0	0	0
CM/CMF-0.3	1500	750	0.5	0.3	4.5	2.28
CM/CMF-0.6	1500	750	0.5	0.6	9.0	4.55
CM/CMF-0.9	1500	750	0.5	0.9	13.5	6.83

* The CO_2 dose percentage is by weight of cement and was selected based on previous studies (Monkman and MacDonald, 2016; Monkman et al., 2016). AM: air-mixing sample; CM: CO_2-mixing samples; CMF: CO_2-mixing with further mixing samples

gas (about 1.977 g/L at atmospheric pressure), and t is the length (min) of CO_2-mixing stage (fixed at 1 min for all cases).

The mixing regime of the cement paste samples is illustrated in Fig. 1. A control sample (AM) was prepared by mixing OPC with water at 140 and 280 r/min for 1 and 2 min, respectively, to obtain a homogeneous state. As for CO_2-mixing (CM) samples, an additional mixing stage of 1 min (280 r/min) was required to allow 0.3%, 0.6%, and 0.9% CO_2 doses to be injected and mixed with the freshly prepared wet cement paste in an enclosed mixer (Fig. 2). Once the mixer was opened, the pastes were highly stiffened and not workable. To investigate the effect of prolonged mixing time, immediately after CO_2-mixing the mixture was further mixed for another 1 min at 280 r/min and labelled the samples CMF-0.3, 0.6, and 0.9. Note that before the second mixing stage, the cover of the enclosed mixer was opened in order to ensure that any unreacted CO_2 was released into the environmental air.

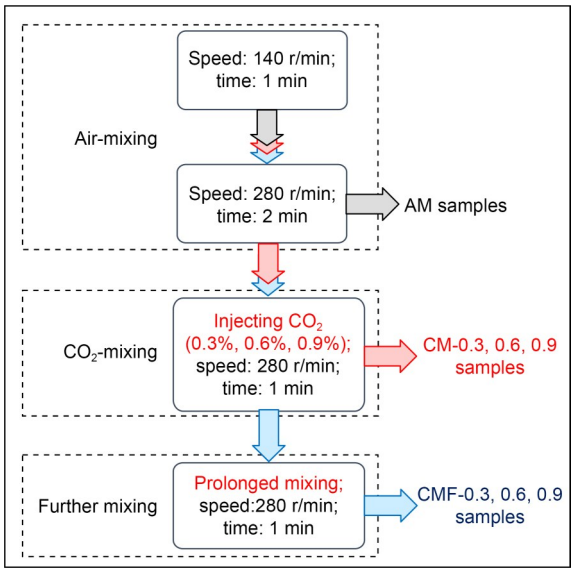

Fig. 1 Mixing regimes designed for CO_2-mixing cement pastes

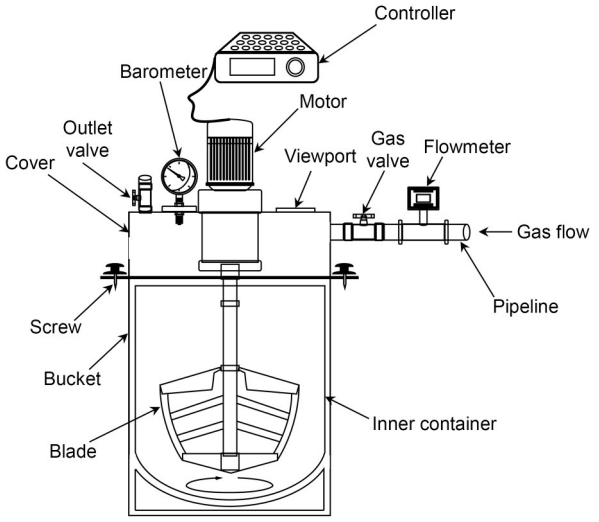

Fig. 2 Schematic diagram of the enclosed (airtight) mixer coupled with a CO_2 injector. The bucket was sealed with a rubber ring on the top and enclosed with four screws at each side. The mixer volume was 10 L, and the mixing speed and CO_2 flow rate could be controlled in the range of 0–400 r/min and 0–10 L/min, respectively

All freshly prepared mixtures were poured into 40 mm×40 mm×40 mm steel molds and vibrated for 20 s. The hardened pastes were demolded after 1 d and then further cured in a standard chamber (relative humidity of 95% and temperature (T) of 20 °C) until the testing ages.

2.3 Testing methods for fresh properties

2.3.1 Flowability

Mini-slump test was used to assess the flowability of the fresh cement paste mixture (Mehdizadeh et al., 2022). A truncated cone with a size of 36 mm×60 mm×60 mm was placed at the center of the flow table and then filled with the freshly prepared mixture. After the cone was lifted vertically, the mixture was dropped 15 times at a rate of one jolt per second. The diameter of the spread mixture in two perpendicular directions was recorded.

2.3.2 Setting time

The initial and final setting times of the fresh cement paste mixture were measured with a Vicat Apparatus in accordance with GB/T 1346 (GAQSIQ, 2012). The needle used was (1.000±0.005) mm in diameter. This test was carried out in the laboratory with a relative humidity of 60% and a room temperature of (20±3) ℃.

2.3.3 Heat of hydration

The exothermal curves of samples were measured according to GB/T 12959 (GAQSIQ, 2008). The paste mixture, with a mass of 10.5 g, was placed into glass ampoules and located into channels of a TAM Air (8-channel) machine (TA Instruments, USA) at 20 ℃ for measurement (up to 7 d). To maintain the heat balance, the reference water was placed in the corresponding channels.

2.3.4 Thermogravimetric analysis (TGA)

The freshly prepared mixture was immersed in isopropyl alcohol to exchange the free water in order to completely stop hydration. For each sample, approximate 15 mg of the powder was used for heating from ambient temperature to 1000 ℃ at a rate of 10 ℃/min under a nitrogen flow of 30 mL/min.

The weight loss x_C at 550–950 ℃ indicates the decomposition of the precipitated $CaCO_3$, as expressed in Eq. (4) (Jiang and Ling, 2020; Ma et al., 2021).

$$x_C = \frac{M_{550} - M_{950}}{M_{950}} \times \frac{100}{44} \times 100\%, \tag{4}$$

where M_{550} and M_{950} are the masses of the sample at given temperature of 550 ℃ and 950 ℃, respectively.

2.3.5 Scanning electron microscopy (SEM)

The SEM observation was performed on oven-dried fresh paste mixture using a JSM-7900F SEM (JEOL, Japan) with an energy dispersive spectrometer (EDS). Samples were coated with a thin conductive layer of gold (Au) to minimize charging.

2.4 Testing methods for hardened properties

2.4.1 Compressive strength

Compressive strength testing was carried out at 1, 3, 7, and 28 d using a conventional compression machine with a loading rate of 2.4 kN/s, according to GB/T 17671 (SBQTS, 1999). The average values of three samples were reported.

2.4.2 Sorptivity and water absorption

The sorptivity and water absorption of samples were measured at 28 d according to ASTM C1585-04 (ASTM, 2004) and ASTM C642-13 (ASTM, 2013), respectively. Samples were first oven dried at 80 ℃ until a constant weight (dry weight, W_1), and then the four sides surfaces of each sample were sealed with waterproof paint (sealed weight, W_2), ensuring that water movement would take place only through the bottom surface. Plastic pipes were used to support the samples so that the water level was kept 5 mm above the bottom surface. Samples were removed from the water and weighed at intervals of 10 min, 20 min, 30 min, 1 h, 2 h, 4 h, 6 h, 12 h, 24 h, and 48 h for measurement. The sorptivity coefficient (S, mm/s$^{1/2}$) was calculated by

$$I = St_1 + b, \tag{5}$$

where I refers to the cumulative volume of absorbed water per unit of water contact area (mm^3/mm^2), t_1 is the time (s), and b is the constant which reflects the effect of initial water filling at the sample surface.

After 48 h, all samples were at constant weight (saturated surface-dry weight, W_3) to attain final water absorption values, as expressed by

$$a = \frac{W_3 - W_2}{W_1} \times 100\%, \tag{6}$$

where a is the final water absorption.

2.4.3 Backscattered electron microscopy (BSE)

Microstructure and porosity of samples at 3 and 28 d were analyzed using a BSE (JSM-IT500, JEOL, Japan). Samples were cut into size of 5 mm×10 mm×10 mm by a low-speed diamond blade. Then, moisture was removed by storing the samples in a vacuum oven at 20 ℃ for 5 d. After that, the samples were impregnated with a low-viscosity epoxy resin (EPO-TEK 301, BUEHLER, Germany) under vacuum conditions. After demolding, the surface of the samples was lapped using SiC papers of 400 and 1200 grit and further polished with oil-based diamond polishing fluid of 5, 2.5, and 1 μm in sequence. To calculate the microporosity, 12 BSE images at 500× magnification were

taken and analyzed with Image J software. A specific threshold with an empirical coefficient of 0.9 was chosen to avoid overestimating porosity based on the cumulative grayscale curve (Lyu et al., 2019; Peng et al., 2020).

2.4.4 Reaction products

The fractured samples derived from the compression tests at 1, 3, 7, and 28 d were immersed in isopropyl alcohol for at least 3 d to stop the hydration process and then vacuum-dried for 5 d before being ground into powder with a size of <75 μm for TGA measurement.

The degree of hydration (α) was calculated according to Eqs. (7) and (8), on the basis of the method proposed by Monteagudo et al. (2014) and Akbar and Liew (2020).

$$W_B = \mathrm{Ldh} + \mathrm{Ldx} + 0.41\mathrm{Ldc}, \tag{7}$$

$$\alpha = \frac{W_B}{0.24}, \tag{8}$$

where Ldh is the dehydration (105–400 °C), Ldx is the dehydroxylation (400–500 °C), and Ldc is the decarbonation (550–950 °C). The value of 0.24 represents the maximum amount of chemically bound water required to hydrate a cement particle entirely.

3 Results and discussion

3.1 Fresh properties

3.1.1 Flowability

The appearance of the cement pastes before and after vibration on the flow table is shown in Fig. 3. As seen, CO_2 induced quick hardening of the paste mixture, which is found to be quite similar to false setting (Chung and Lee, 2011; Liu, 2019). The values of mini-slump flow of CM samples were about 31.3%, 43.1%, and 45.9% lower compared with the AM sample with increased CO_2-mixing doses of 0.3%, 0.6%, and 0.9%, respectively. This was due to the $CaCO_3$ deposited on cement particles increasing the specific surface area and thus absorbing more free water (Liu et al., 2012; Cui et al., 2021).

It is important to note that with an additional 1 min of high-speed mixing, CMF samples showed improved workability. The specific recovery rates were 52.8%, 80.6%, and 84.9% for the 0.3%, 0.6%, and 0.9% CO_2-mixing samples, respectively. The resulting flowability of CMF samples (140.5–147.5 mm) was even slightly higher (~5%) than that of the control AM sample. This is because the increased mixing time increases collisions between particles, inducing detachment of $CaCO_3$ which induces the balling effect and creating a lubricating layer between particles (Camiletti et al., 2013).

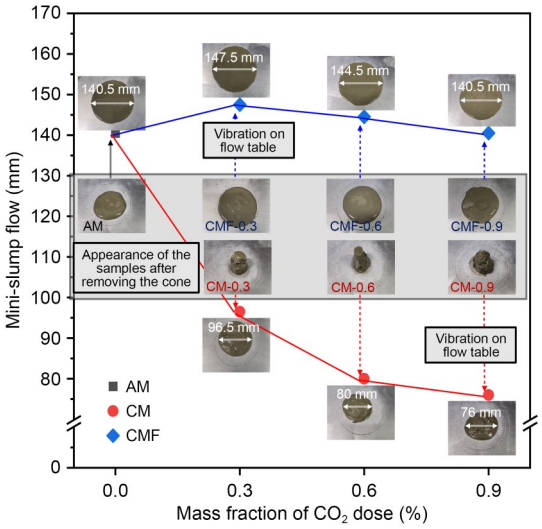

Fig. 3 Physical appearance and mini-slump flow values of the freshly prepared CO_2-mixing pastes

3.1.2 Setting time

The initial and final setting times of the cement pastes are presented in Fig. 4. The initial setting times for CM samples were 10–40 min shorter than that of the AM sample, due to the quick hardening behavior of the cement matrix. In comparison, the initial setting times for CMF samples were prolonged for 20–66 min compared to the AM sample, because of the breakup of the flocculation and release of free water.

The final setting times of CM samples and CMF samples were generally shortened compared with the AM sample, at approximately 140 min and 65 min, respectively. This was attributed to the promotion of hydration by the presence of $CaCO_3$, which led to a faster final setting time. In addition, it is worth noting that the interval between initial and final setting times of CO_2-mixing pastes was significantly shortened compared with the AM sample (from 236 min to 80–150 min), which demonstrated the potential of CO_2-mixing to provide strength for building construction in a faster and greener way (Guo et al., 2020).

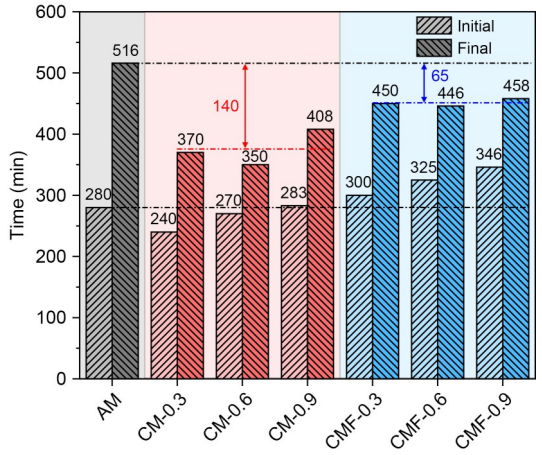

Fig. 4 Initial and final setting times of cement pastes

3.1.3 Heat of hydration

The isothermal calorimetry results of AM and CMF samples (up to 7 d) are presented in Fig. 5. The calorimetry slope increased with CO_2-mixing dose for the first 6 h, indicating an acceleration of the primary hydration peak of C_3S due to the presence of CO_2. However, the intensity of the first hydration peak was slightly lower (~6%–8%) than for the AM sample, because some of the C_3S was consumed by CO_2 during the mixing process. These results are consistent with those reported by Monkman et al. (2020), who found that C_3S was the main reactant of the CO_2-mixing process due to the absence of hydration products at the most initial hydration stage.

The second peak intensity was higher and the cumulative heat at 72 h for the higher CO_2-mixing dose samples was higher than those of the CMF-0.3 and AM samples (Fig. 5b). This was due to the formation of $CaCO_3$, which promotes aluminate hydration. However, this promotion became insignificant at a later age of 7 d. In addition, the thermal indicator of setting time reflected in the hydration heat flow (according to ASTM C1679 (ASTM, 2014)) of the CMF-0.3, 0.6, and 0.9 samples was shortened by about 29, 46, and 52 min, respectively, compared to the AM sample (Haha et al., 2010; Monkman et al., 2018). This matched the setting time measurements given in Section 3.1.2.

3.1.4 Thermogravimetric analysis

The results of the TGA for fresh cement pastes are illustrated in Fig. 6. It is notable that the peaks for hydration products (i.e., C–S–H and ettringite) are generally increased for the case of CO_2-mixing samples

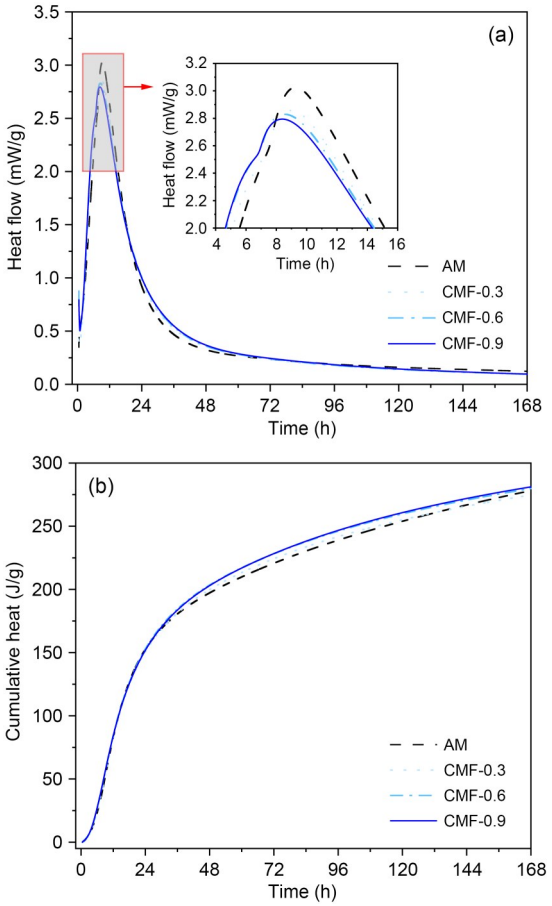

Fig. 5 Heat flow (a) and cumulative heat (b) over time for AM and CMF-0.3, 0.6, and 0.9 samples. The CM samples were excluded due to their quick hardening behavior. References to color refer to the online version of this figure

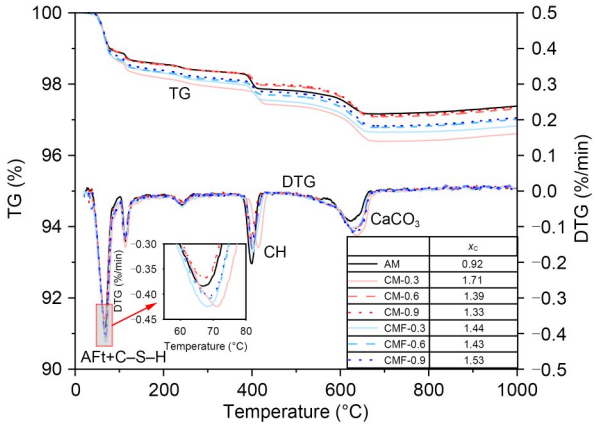

Fig. 6 Derivative thermogravimetric curve (DTG) and thermalgravimetric (TG) curves of freshly prepared cement pastes. References to color refer to the online version of this figure

due to the hydration-promotion effects of $CaCO_3$. As expected, the $Ca(OH)_2$ content in all the CO_2-mixing

cement pastes was lower than that in AM paste, because more $CaCO_3$ was precipitated. The calculation of the $CaCO_3$ content of each sample is shown in Fig. 6. It can be seen that the CM-0.3 sample had the highest $CaCO_3$ content, which may be related to the continuous dissolution of CO_2 in the water at a relative low flow rate. When the CO_2 dose was higher than 0.6%, the mixture became less workable due to the fact that most of the free water was entrapped by the flocculation networks. Moreover, CO_2 could no longer dissolve into water. Upon further mixing, the entrapped water was released and clinkers had better contact with CO_2. In addition, it can be seen that the endothermal peaks of $CaCO_3$ in all the CM and CMF samples shifted toward a slightly higher temperature compared to the AM paste, indicating that more crystalline $CaCO_3$ was formed in the pastes matrix.

3.1.5 Morphology of the fresh cement pastes

Fig. 7 compares the morphologies of AM, CM-0.6, and CMF-0.6 samples. It is clear that the surface of the AM sample was plain and neat. However, an abundance of flocculated hydration and carbonation products was deposited on the cement particles of the fresh CM-0.6 sample (Fig. 7b). The EDS spectra of spots 1 and 2 showed that the flocculated phases mainly consisted of C–S–H gels, and probably of amorphous calcium carbonate (with a relatively high content of C element). The deposited $CaCO_3$ on the surface of cement particles could interact with flowing suspended particles, which led to the so-called interlocking effect; this decreased flowability (Cao et al., 2019). Furthermore, $CaCO_3$ also acted as a nucleation site to accelerate cement hydration, leading to the formation of more reaction products on the surface layer of clinker particles (Monkman et al., 2020). As a result, more water was needed to wet the larger specific surface area of the solid particles. Upon further mixing for 1 min, the surface of these particles became smoother, with only some amorphous calcium carbonate (spot 3) instead of flocculated phases. This demonstrated that further mixing helped to destroy the flocculation network and release the entrapped free water.

3.2 Hardened properties

3.2.1 Compressive strength

The compressive strength results at 1, 3, 7, and 28 d are presented in Fig. 8. For all CM samples, the compressive strength was about 10%–20% lower than that of the control AM sample at the same curing age, which is consistent with the results found by Monkman and MacDonald (2016). This is probably due to the poor workability which caused the fresh pastes too stiffer to be fully compacted and left air pores in the matrix. Adding 1 min of mixing time immediately after CO_2 mixing resulted in distinct improvements in compressive strength compared to the corresponding CM samples. This could be primarily due to the improved workability and nucleation sites effect of the break-up deposited calcium carbonate in accelerating early hydration (He et al., 2017; Monkman et al., 2020; Dixit et al., 2021, 2022). In comparison, the rate at which strength improved (~18%–32%) was more pronounced for the cement-paste samples with low (CMF-0.3) and moderate (CMF-0.6) CO_2-mixing. At a later age (28 d), the compressive strength of CMF samples was comparable to that of AM samples because the positive effect of $CaCO_3$ as a nucleation site became less important (Luo et al., 2022). The relatively low compressive strength of the CMF-0.9 sample was attributed to the larger pore structure induced by an excessive dose of CO_2, as will be discussed in the following section.

3.2.2 Sorptivity and water absorption

Fig. 9a shows the cumulative amount of water absorbed per unit area over the square root of time; the sorptivity coefficients (i.e., the slopes of the initial line fitting) are listed in Table 4, and are useful in terms of reflecting the capillary pores of the samples (Wang et al., 2022; Zhang et al., 2022). The CMF samples had a higher water sorptivity rate than the control AM and CM samples at the first 12 h, indicating that more connected pores had formed in the paste matrix. For instance, damp patches could be clearly seen on the top surface of the CMF-0.6 sample, unlike the corresponding CM-0.6 sample. It should be noted that the CM-0.9 sample had a relatively low sorptivity coefficient compared to other samples, probably because of a larger pore size in the matrix (Fig. 10a), composed mainly of closed air pores rather than connected ones.

The final water-absorption values of CMF samples (measured at 48 h of full water immersion) were about 6%–11% lower than those of CM samples, and CMF-0.9 had the highest value. As the porosity of a paste matrix determines its compressive strength, it is

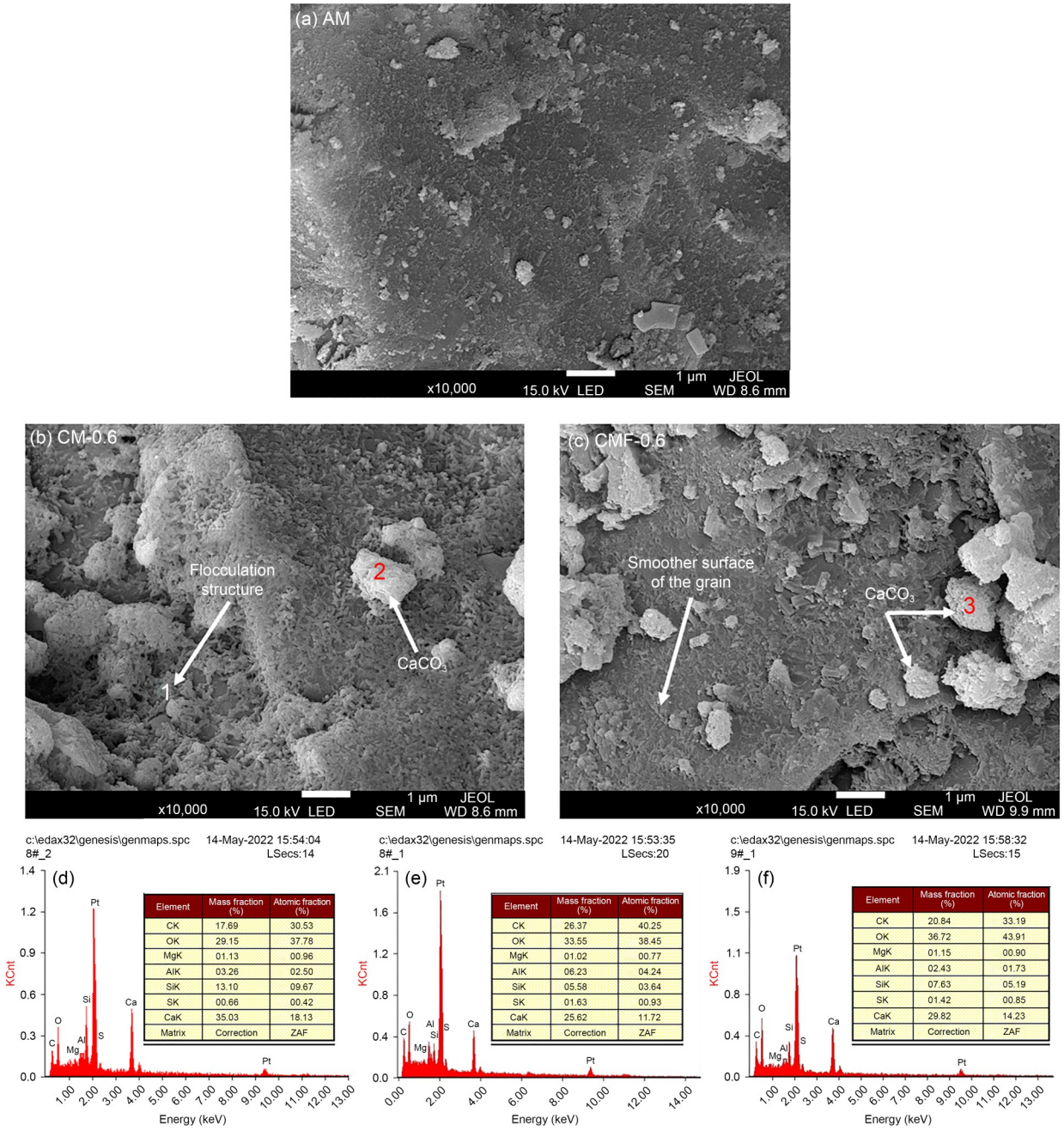

Fig. 7 Morphologies of the freshly prepared CO_2-mixing cement pastes of AM (a), CM-0.6 (b), and CMF-0.6 (c), and EDS spectra of spot 1 (d), spot 2 (e), and spot 3 (f)

of interest to plot the final water absorption as a function of compressive strength. The final water-absorption values appeared to be well correlated with the compressive strength results at 28 d (Fig. 9b). This statistical relation suggested that the lower the final water absorption, the higher the compressive strength of the samples, regardless of the CO_2-mixing dose or mixing approach.

3.2.3 Porosity analysis

An optical microscope and BSE were also used for close examination of the effects of CO_2-mixing dose and further mixing time on the pore structures of the investigated samples. Fig. 10 shows that the pore size and the amount of pores appearing on the surface of the CM samples increased with higher CO_2-mixing

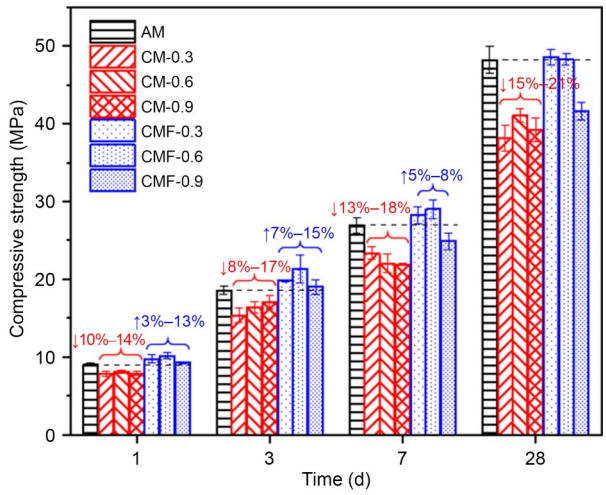

Fig. 8 Compressive strength of hardened cement pastes over time

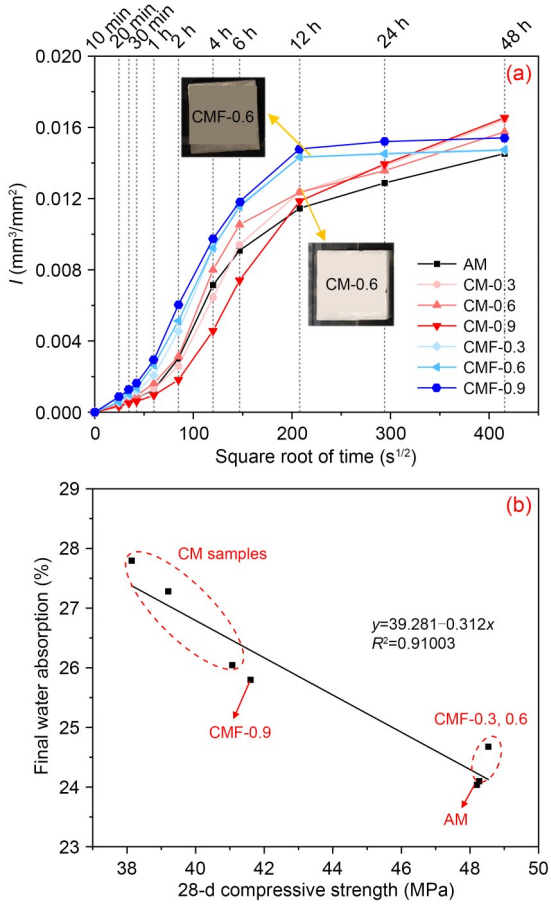

Fig. 9 Water sorptivity of CO_2-mixing cement pastes over time (a) and relationship between 28-d compressive strength and final water absorption (b)

doses. This is understandable considering their low workability, which resulted in poor compacting and

Table 4 Sorptivity coefficients (S) of the CO_2-mixing cement pastes

Sample	S ($\times10^{-5}$ mm/s$^{1/2}$)	Sample	S ($\times10^{-5}$ mm/s$^{1/2}$)
AM	6.63	CMF-0.3	8.53
CM-0.3	6.50	CMF-0.6	8.50
CM-0.6	7.56	CMF-0.9	8.76
CM-0.9	4.93		

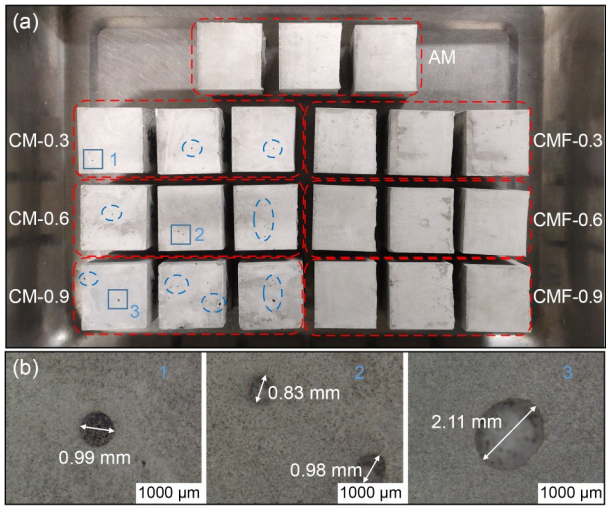

Fig. 10 Appearance of samples at 28 d (a) and pore sizes (b)

formation of cavities in the pastes. It is also congruent with the higher final water absorption and lower compressive strength of CM samples presented in Fig. 9b.

Table 5 shows the BSE porosity values of AM, CM-0.6, and CMF-0.6 samples, and the details of the porosity calculation and respective sample images are listed in Figs. S1 and S2 in the electronic supplementary materials (ESM). At 3 d, both the CM-0.6 and CMF-0.6 samples exhibited lower porosity than the control AM sample, in agreement with previous studies which reported that the presence of calcite in the cement matrix can promote early hydration and densify the microstructure (Monkman and MacDonald, 2016; Monkman et al., 2020). It is clear that the pore structure of all samples was refined over time (from 3 to 28 d) due to more complete hydration in the pastes. In comparison, the reduction of pore structure in the control sample (AM) was greater than those CO_2-mixing samples. This implies that the presence of calcite may not be beneficial for porosity refinement during hydration.

Table 5 Calculated porosity of AM, CM-0.6, and CMF-0.6 samples at 3 d and 28 d

Time (d)	Calculated porosity (%)		
	AM	CM-0.6	CMF-0.6
3	12.15	11.63	10.55
28	7.79	10.94	9.56

3.2.4 Reaction products of the hardened stage

Fig. 11a shows the evolution of $CaCO_3$ formation in CO_2-mixing cement pastes over hydration time (up to 28 d). The $CaCO_3$ content increased with time at early ages (≤7 d), possibly due to the dissolved CO_2 in the pore solution leading to precipitation of $CaCO_3$. However, $CaCO_3$ content decreased at 28 d because it reacted with tricalcium aluminate (C_3A) and/or monosulfate (AFm) to form hemi-carbonaluminate (Hc) and mono-carbonaluminate (Mc) (Zajac et al., 2014; Ren et al., 2022) (Fig. S3). In general, the CM samples had a higher content of $CaCO_3$ than the control AM and CMF samples, because part of the injected CO_2 gas was released during the further mixing of 1 min.

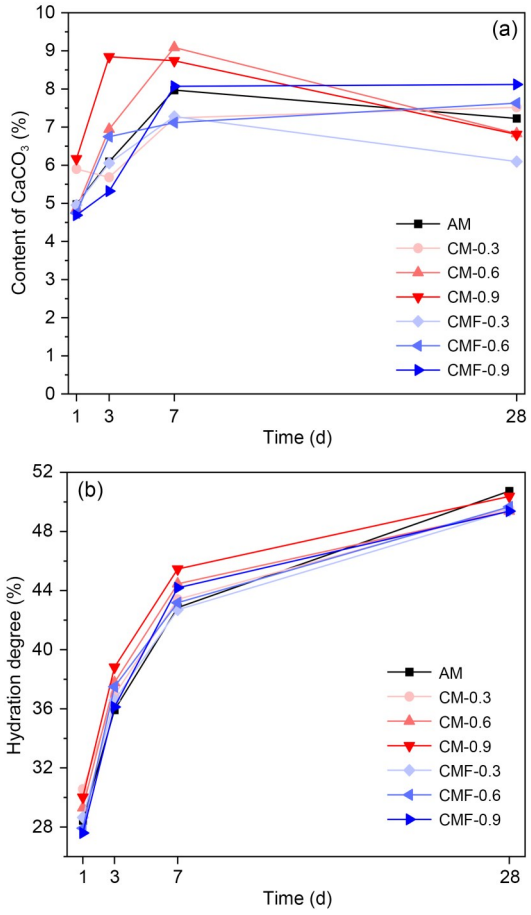

Fig. 11 The amount of $CaCO_3$ detected in CO_2-mixing cement pastes (a) and evolution of hydration degree over different hydration times (b)

The evolution of hydration degree over hydration time is plotted in Fig. 11b. At early ages (≤7 d), the hydration degree of both CM and CMF samples was generally higher than that of the control AM sample. In comparison, CM samples possessed a relatively higher hydration degree than CMF samples for a given CO_2 dose and curing age. This is due to a higher amount of actual reacted CO_2 promoting better cement hydration in CM samples. However, CM samples had a relatively low compressive strength, due to the poor compactness and larger pores associated with their lower workability. The AM sample displayed the highest hydration degree at 28 d, in line with the BSE porosity results (Table 5), proving that CO_2 mixing of the fresh cement paste only can promote early cement hydration.

4 Conclusions

In this study, the influence of CO_2 dose applied during mixing of cement pastes, as well as subsequent further mixing, on fresh and hardened properties of cement pastes was investigated. At the fresh stage, the introduction of CO_2-mixing induces quick hardening, and flowability decreases dramatically with higher CO_2 doses. This is mainly associated with the flocculation network by the formation of hydrates and carbonates on the surface of the cement clinkers. However, with 1 min of further mixing, the workability of fresh cement pastes can be improved by 52.8%–84.9% because this breaks up the flocculation network and releases entrapped free water.

In terms of compressive strength, a direct CO_2-mixing results in a ~10%–20% compressive strength loss at all curing ages, despite a higher degree of hydration. This is because of the poor compaction of the fresh cement mixture, which induces development of a more extensive pore structure in the hardened matrix. However, upon 1 min of further mixing, the overall compressive strength is enhanced by ~18%–32%, and demonstrated an early strength benefit of 3%–15% compared to the control sample. This is due to the hydration-promoting effect of the deposited $CaCO_3$ and a more densified microstructure. In addition, a strong

linear correlation between 28-d compressive strength and water absorption was observed, indicating that pore distribution plays an important role in the alteration of strength for CO_2-mixing cement pastes.

Acknowledgments

This work is supported by the Science and Technology Innovation Plan of Hunan Province (No. 2022WZ1010) and the Program Fund of Non-Metallic Excellence and Innovation Center for Building Materials (No. 2023Ph.D-6), China.

Author contributions

Minlu WANG designed the research, processed the corresponding data, and wrote the first draft of the manuscript. Shuang LUO and Ba Tung PHAM helped to organize the manuscript. Tung-Chai LING revised and edited the final version.

Conflict of interest

The authors declare that they have no known competing financial interests or personal relationships that could have influenced the work reported in this paper.

References

Akbar A, Liew KM, 2020. Influence of elevated temperature on the microstructure and mechanical performance of cement composites reinforced with recycled carbon fibers. *Composites Part B: Engineering*, 198:108245. https://doi.org/10.1016/j.compositesb.2020.108245

Ashraf W, 2016. Carbonation of cement-based materials: challenges and opportunities. *Construction and Building Materials*, 120:558-570. https://doi.org/10.1016/j.conbuildmat.2016.05.080

ASTM (American Society for Testing Materials), 2004. Standard Test Method for Measurement of Rate of Absorption of Water by Hydraulic-Cement Concretes, ASTM C1585-04. ASTM, USA.

ASTM (American Society for Testing Materials), 2013. Standard Test Method for Density, Absorption, and Voids in Hardened Concrete, ASTM C642-13. ASTM, USA.

ASTM (American Society for Testing Materials), 2014. Standard Practice for Measuring Hydration Kinetics of Hydraulic Cementitious Mixtures using Isothermal Calorimetry, ASTM C1679. ASTM, USA.

Berger RL, Young JF, Leung K, 1972. Acceleration of hydration of calcium silicates by carbon dioxide treatment. *Nature*, 240(97):16-18.

Camiletti J, Soliman AM, Nehdi ML, 2013. Effects of nano- and micro-limestone addition on early-age properties of ultra-high-performance concrete. *Materials and Structures*, 46(6):881-898. https://doi.org/10.1617/s11527-012-9940-0

Cao ML, Ming X, He KY, et al., 2019. Effect of macro-, micro- and nano-calcium carbonate on properties of cementitious composites–a review. *Materials*, 12(5):781. https://doi.org/10.3390/ma12050781

Chung CW, Lee JY, 2011. Premature stiffening of cement paste caused by secondary gypsum and syngenite formation (false set). *Architectural Research*, 13(1):25-32. https://doi.org/10.5659/aikar.2011.13.1.25

Cui K, Lau D, Zhang YY, et al., 2021. Mechanical properties and mechanism of nano-$CaCo_3$ enhanced sulphoaluminate cement-based reactive powder concrete. *Construction and Building Materials*, 309:125099. https://doi.org/10.1016/j.conbuildmat.2021.125099

Dixit A, Du HJ, Pang SD, 2021. Carbon capture in ultra-high performance concrete using pressurized CO_2 curing. *Construction and Building Materials*, 288:123076. https://doi.org/10.1016/j.conbuildmat.2021.123076

Dixit A, Geng GQ, Du HJ, et al., 2022. The role of age on carbon sequestration and strength development in blended cement mixes. *Cement and Concrete Composites*, 133: 104644. https://doi.org/10.1016/j.cemconcomp.2022.104644

GAQSIQ (General Administration of Quality Supervision, Inspection and Quarantine of the People's Republic of China), 2008. Test Methods for Heat of Hydration of Cement, GB/T 12959-2008. National Standards of the People's Republic of China (in Chinese).

GAQSIQ (General Administration of Quality Supervision, Inspection and Quarantine of the People's Republic of China), 2012. Test Methods for Water Requirement of Normal Consistency, Setting Time and Soundness of the Portland Cement, GB/T 1346-2011. National Standards of the People's Republic of China (in Chinese).

Guo JF, Wang L, Fan KP, et al., 2020. An efficient model for predicting setting time of cement based on broad learning system. *Applied Soft Computing*, 96:106698. https://doi.org/10.1016/j.asoc.2020.106698

Haha MB, de Weerdt K, Lothenbach B, 2010. Quantification of the degree of reaction of fly ash. *Cement and Concrete Research*, 40(11):1620-1629. https://doi.org/10.1016/j.cemconres.2010.07.004

Han D, Ferron RD, 2015. Effect of mixing method on microstructure and rheology of cement paste. *Construction and Building Materials*, 93:278-288. https://doi.org/10.1016/j.conbuildmat.2015.05.124

Han D, Ferron RD, 2016. Influence of high mixing intensity on rheology, hydration, and microstructure of fresh state cement paste. *Cement and Concrete Research*, 84:95-106. https://doi.org/10.1016/j.cemconres.2016.03.004

He Z, Li Z, Shao YX, 2017. Effect of carbonation mixing on CO_2 uptake and strength gain in concrete. *Journal of Materials in Civil Engineering*, 29(10):04017176. https://doi.org/10.1061/(ASCE)MT.1943-5533.0002031

Hossain M, Rashid H, Mahmud F, 2018. Effects of continuous mixing on mechanical problems of concrete. Proceedings of the 4th International Conference on Civil Engineering for Sustainable Development, article 4515.

Jiang Y, Ling TC, 2020. Production of artificial aggregates from steel-making slag: influences of accelerated carbonation during granulation and/or post-curing. *Journal of CO_2 Utilization*, 36:135-144. https://doi.org/10.1016/j.jcou.2019.11.009

Kwasny J, Basheer PAM, Russell MI, 2014. CO_2 sequestration in cement-based materials during mixing process using carbonated water and gaseous CO_2. Proceedings of the 4th International Conference on Durability of Concrete Structures, p.72-79. https://doi.org/10.5703/1288284315385

Li YS, Mehdizadeh H, Mo KH, et al., 2023. Co-utilization of aqueous carbonated basic oxygen furnace slag (BOFS) and carbonated filtrate in cement pastes considering reaction duration effect. *Cement and Concrete Composites*, 138:104988. https://doi.org/10.1016/j.cemconcomp.2023.104988

Lippiatt N, Ling TC, 2020. Rapid hydration mechanism of carbonic acid and cement. *Journal of Building Engineering*, 31:101357. https://doi.org/10.1016/j.jobe.2020.101357

Lippiatt N, Ling TC, Eggermont S, 2019. Combining hydration and carbonation of cement using super-saturated aqueous CO_2 solution. *Construction and Building Materials*, 229:116825. https://doi.org/10.1016/j.conbuildmat.2019.116825

Liu LL, Ji YS, Gao FR, et al., 2021. Study on high-efficiency CO_2 absorption by fresh cement paste. *Construction and Building Materials*, 270:121364. https://doi.org/10.1016/j.conbuildmat.2020.121364

Liu XY, 2019. Research of the Hydration and Hardening Mechanism of Cement-Based Materials after Absorbing CO_2 in Mixing Stage. MS Thesis, China University of Mining and Technology, China (in Chinese).

Liu XY, Chen L, Liu AH, et al., 2012. Effect of nano-$CaCO_3$ on properties of cement paste. *Energy Procedia*, 16:991-996. https://doi.org/10.1016/j.egypro.2012.01.158

Luo S, Guo MZ, Ling TC, 2022. Mechanical and microstructural performances of fly ash blended cement pastes with mixing CO_2 during fresh stage. *Construction and Building Materials*, 358:129444. https://doi.org/10.1016/j.conbuildmat.2022.129444

Lyu K, She W, Miao CW, et al., 2019. Quantitative characterization of pore morphology in hardened cement paste via SEM-BSE image analysis. *Construction and Building Materials*, 202:589-602. https://doi.org/10.1016/j.conbuildmat.2019.01.055

Ma MT, Mehdizadeh H, Guo MZ, et al., 2021. Effect of direct carbonation routes of basic oxygen furnace slag (BOFS) on strength and hydration of blended cement paste. *Construction and Building Materials*, 304:124628. https://doi.org/10.1016/j.conbuildmat.2021.124628

Mehdizadeh H, Cheng XF, Mo KH, et al., 2022. Upcycling of waste hydrated cement paste containing high-volume supplementary cementitious materials via CO_2 pre-treatment. *Journal of Building Engineering*, 52:104396. https://doi.org/10.1016/j.jobe.2022.104396

Mehdizadeh H, Mo KH, Ling TC, 2023. CO_2-fixing and recovery of high-purity vaterite $CaCO_3$ from recycled concrete fines. *Resources, Conservation and Recycling*, 188:106695. https://doi.org/10.1016/j.resconrec.2022.106695

Monkman S, MacDonald M, 2016. Carbon dioxide upcycling into industrially produced concrete blocks. *Construction and Building Materials*, 124:127-132. https://doi.org/10.1016/j.conbuildmat.2016.07.046

Monkman S, MacDonald M, 2017. On carbon dioxide utilization as a means to improve the sustainability of ready-mixed concrete. *Journal of Cleaner Production*, 167:365-375. https://doi.org/10.1016/j.jclepro.2017.08.194

Monkman S, MacDonald M, Hooton RD, et al., 2016. Properties and durability of concrete produced using CO_2 as an accelerating admixture. *Cement and Concrete Composites*, 74:218-224. https://doi.org/10.1016/j.cemconcomp.2016.10.007

Monkman S, Kenward PA, Dipple G, et al., 2018. Activation of cement hydration with carbon dioxide. *Journal of Sustainable Cement-Based Materials*, 7(3):160-181. https://doi.org/10.1080/21650373.2018.1443854

Monkman S, Lee BEJ, Grandfield K, et al., 2020. The impacts of in-situ carbonate seeding on the early hydration of tricalcium silicate. *Cement and Concrete Research*, 136:106179. https://doi.org/10.1016/j.cemconres.2020.106179

Monteagudo SM, Moragues A, Gálvez JC, et al., 2014. The degree of hydration assessment of blended cement pastes by differential thermal and thermogravimetric analysis. Morphological evolution of the solid phases. *Thermochimica Acta*, 592:37-51. https://doi.org/10.1016/j.tca.2014.08.008

Peng Y, Zeng Q, Xu SL, et al., 2020. BSE-IA reveals retardation mechanisms of polymer powders on cement hydration. *Journal of the American Ceramic Society*, 103(5): 3373-3389. https://doi.org/10.1111/jace.16982

Ren PF, Ling TC, Mo KH, 2022. CO_2 pretreatment of municipal solid waste incineration fly ash and its feasible use as supplementary cementitious material. *Journal of Hazardous Materials*, 424:127457. https://doi.org/10.1016/j.jhazmat.2021.127457

SBQTS (The State Bureau of Quality and Technical Supervision), 1999. Method of Testing Cements–Determination of Strength, GB/T 17671-1999. National Standards of the People's Republic of China (in Chinese).

Urban K, Sicakova A, 2018. The effect of mixing technique and prolonged mixing time on strength characteristics of concrete. *Proceedings*, 2(20):1290. https://doi.org/10.3390/proceedings2201290

Wang Y, Li LS, An MZ, et al., 2022. Factors influencing the capillary water absorption characteristics of concrete and their relationship to pore structure. *Applied Sciences*, 12(4): 2211. https://doi.org/10.3390/app12042211

Zajac M, Rossberg A, le Saout G, et al., 2014. Influence of limestone and anhydrite on the hydration of Portland cements. *Cement and Concrete Composites*, 46:99-108. https://doi.org/10.1016/j.cemconcomp.2013.11.007

Zhang CY, Zhang SF, Yu JW, et al., 2022. Water absorption behavior of hydrophobized concrete using silane emulsion as admixture. *Cement and Concrete Research*, 154: 106738. https://doi.org/10.1016/j.cemconres.2022.106738

Zhang D, Ghouleh Z, Shao YX, 2017. Review on carbonation curing of cement-based materials. *Journal of CO_2 Utilization*, 21:119-131. https://doi.org/10.1016/j.jcou.2017.07.003

Zhao KY, Zhao LJ, Zhang XB, et al., 2022. An experimental study on the mixing process and properties of concrete based on an improved three-stage mixing approach. *Materials and Structures*, 55(5):134. https://doi.org/10.1617/s11527-022-01976-y

Electronic supplementary materials

Figs. S1–S3